Supporting Information for

Escherichia coli Dihydrofolate Reductase Catalyzed Proton and Hydride Transfers: Temporal Order and the Roles of Asp27 and Tyr100

Classification: *Biological Sciences*: Biochemistry

Authors: C. Tony Liu[†‡], Kevin Francis[⊥‡], Joshua Layfield[^], Xinyi Huang[†], Sharon Hammes-Schiffer[^], Amnon Kohen[⊥*] and Stephen J. Benkovic[†*]

Affiliations:

[†]Department of Chemistry, Pennsylvania State University, University Park, PA 16802, USA.

[⊥] Department of Chemistry, The University of Iowa, Iowa City, IA 52242.

[^]Department of Chemistry, University of Illinois at Urbana-Champaign, Urbana, IL 61801-3364, USA.

[‡]These authors contributed equally to this work.

* To Whom Correspondence should be addressed. E-mails: Amnon-kohen@uiowa.edu (A.K.), sjb1@psu.edu (S.J.B.).

Contents

1. Materials and Methods

1.1 Materials. [Carbonyl-^{14}C]-nicotinamide containing a specific radioactivity of > 220 mCi/mol was obtained from Perkin Elmer. 7,8-Dihydrofolate (DHF) was synthesized through the reduction of folic acid with dithionite using a previously described procedure.(3) Glucose dehydrogenase from *Bacillus megaterium* was purchased from Affymetrix/USB, while all other enzymes used in the synthesis of radio-labeled substrates were from Sigma-Aldrich. [Carbonyl-^{14}C]-NADPH, (*R*)-[4-^{3}H]-NADPH (NADPT) and (*R*)-[4-^{2}H]-NADPH (NADPD) were prepared and purified according to previously published procedures.(4) *β*-Nicotinamide adenine dinucleotide phosphate reduced tetra(cyclohexylammonium) salt (NADPH), *β*-Nicotinamide adenine dinucleotide phosphate hydrate ($NADP^+$), 4-(2-hydroxyethyl)-1-piperazineethanesulfonic acid (HEPES), 2-(N-morpholino)ethanesulfonic acid (MES), 2-amino-2-hydroxymethyl-propane-1,3-diol (Tris), methotrexate-agarose, dithiothreitol (DTT), and ethanolamine were purchased from Sigma-Aldrich and used without further purification. pH values were measured using an Accumet model 13-620-300 standard combination electrode calibrated with VWR certified standard aqueous buffers (pH = 4, 7, 10). The pD (D_3O^+ concentrations) values were calculated as pD = pH (electrode reading) + 0.4.(5)

1.2 Kinetics The basic procedures used for the stopped flow measurements are described in the main text. It is important to note that by keeping the [E:NADPH] constant, varying the [DHF] (3 – 100 μM) did not alter the observed rate, suggesting that the values measured are indeed the unimolecular conversion from the ternary E:NADPH:DHF to the product E:$NADP^+$:THF complex. The unchanged kinetic rate constant observed in going from multiple

turnover conditions to single turnover conditions also confirmed that we were indeed measuring the conversion of the ternary complex to the product complex, especially with the absence of a burst kinetic step (faster event) under multiple turnover conditions. This was true across the experimental pL range, as well as when NADPD was replaced by NADPH. This means that the rate constant measurements were determined under full saturation conditions, and the binding of DHF to the binary E:NADPH complex was much faster than the observed reduction of DHF. This simplifies the analysis and avoids kinetic complications that would be associated with the pre-equilibrium binding to generate the reactive E:NADPH:DHF complex.

1.3 pL/ rate profiles. For WT *ec*DHFR with NADPH, with an expanded pL range (5.1-12), the pL rate profiles exhibit a sigmoidal shape defined by plateaus in the low and high pL domains. The pL rate profiles for the hydride transfer step (k_{hyd}) were fit to Eq. S1, which is derived from a scheme that involves two parallel pathways separated by one ionization event (Figure 3).

$$\log(k_{hyd}) = \log\left(k_1 \frac{[H^+]}{K_a + [H^+]} + k_2 \frac{K_a}{K_a + [H^+]} \right) \qquad \text{(S1)}$$

The k_1 and k_2 terms represent the hydride transfer rate constants in the low and high pL plateau, respectively. K_a is the ionization constant that separates k_1 and k_2. The $[H^+]$ is replaced by $[D^+]$ for the rate vs. pD experiments. Eq 1 simplifies to the standard pK_a expression(6) when k_2 is insignificant or under limited experimental pL range. For the *ec*DHFR mutants, the pL rate profiles were fit to a standard linear expression to determine the slopes of the correlations.

1.3 Competitive KIE. Data were collected as described in the main text. Observed KIEs were calculated from that data using Eq. S2:(7)

$$KIE = \frac{\ln(1-f)}{\ln[1-f*(R_t/R_\infty)]} \quad \text{(S2)}$$

where the ratio of ^{14}C in the product and total ^{14}C determined the fractional conversion (*f*), and R_t and R_∞ are the ratio of $^{3}H/^{14}C$ at each time point and at infinite time, respectively. Intrinsic KIEs were calculated from the observed values as previously described,(8-10) using a numerical solution of the modified Northrop equation (Eq. S3):(8, 11)

$$\frac{^{T}(V/K)^{-1}_{H_{obs}} - 1}{^{T}(V/K)^{-1}_{D_{obs}} - 1} = \frac{(k_H/k_T)^{-1} - 1}{(k_H/k_T)^{-1/3.34} - 1} \quad \text{(S3)}$$

where $^{T}(V/K)_{Hobs}$ and $^{T}(V/K)_{Dobs}$ are the observed H/T and D/T KIEs, respectively, and k_H/k_T represents the intrinsic H/T KIE. The intrinsic KIEs and their experimental errors were calculated from all possible combinations of observed H/T and D/T values as described previously.(8, 10) Isotope effects on the activation parameters for the intrinsic KIEs were calculated through a nonlinear fit of all intrinsic values to the Arrhenius equation (Eq. S4):

$$k_l/k_h = A_l/A_h \cdot e^{\Delta E_{a_{h-l}}/RT} \quad \text{(S4)}$$

where k_l and k_h are the rates for light and heavy isotopes, respectively, A_l/A_h is the isotope effect on the Arrhenius pre-exponential factor, $\Delta E_{a\,h-l}$ is the difference in energy of activation between the two isotopes, *R* is the gas constant, and *T* is the absolute temperature.

1.4 Molecular Dynamics Methods. For all MD simulations, we used the AMBER99SB force field to define the potential energy and forces for all of the protein residues(12-13) and the TIP3P(14) potential to describe the water molecules. The bonded and van der Waals parameters for the NADPH cofactor and the DHF and DHF-H^+ substrates were obtained from the

generalized AMBER force field.(15) The partial charges for all three ligands and the deprotonated tyrosine residue were derived using the restrained electrostatic potential method.(16) The partial charges for the protonated and deprotonated form of DHF are presented in Table S10.

Initial coordinates for all of the MD simulations were obtained from the 1RX2 crystal structure,(17) which was solved with the oxidized form of the cofactor bound and folate bound in the substrate binding pocket. The Michaelis complex was simulated by replacing the substrate (FOL) with DHF-H^+ by aligning the corresponding heavy atoms with FOL and replacing the oxidized form of the cofactor ($NADP^+$) by aligning the corresponding heavy atoms with NADPH. The positions of the ligand atoms were optimized with the enzyme and the crystallographic waters held fixed using the steepest-descent algorithm implemented in GROMACS.

After ligand placement and optimization, separate structures with DHF-H^+ bound in the substrate binding pocket and either protonated or deprotonated Tyr100 systems were solvated in TIP3P water molecules inside a truncated octahedral box with sides at least 1.0 nm from the closest enzyme, ligand, or crystallographic water molecule. The system was neutralized by adding either 11 or 12 sodium atoms using the *genion* utility in GROMACS. The solvent molecules and counter ions were then optimized using a steepest-descent algorithm with the enzymatic system held fixed. After optimization, the solvent molecules and counterions were equilibrated in the canonical (constant NVT) ensemble at 300K for 50 ps with the enzyme and ligands held fixed. After the solvent and ions were equilibrated, the entire system was optimized with the steepest-descent algorithm.

After system optimization, the enzyme was subjected to a simulated annealing procedure, where initial velocities were sampled from a Boltzmann distribution at 50 K and then an MD trajectory was propagated for 50 ps at 50 K in the constant NPT ensemble. The temperature was then increased in increments of 50 K and equilibrated at each temperature for 50 ps up to 300 K. Subsequently, each system was equilibrated for an additional 1 ns in the constant NPT ensemble and an additional 1 ns in the canonical (NVT) ensemble. For all of the equilibration MD simulations, the temperature was maintained using the Nose-Hoover thermostat,(18-19) and the Parinello-Rahman barostat(20) was used to maintain the pressure for the simulations in the isothermal-isobaric ensemble (constant NPT). Production trajectories were propagated with a time step of 1 fs, and the temperature was maintained using the leap-frog stochastic dynamics integrator.(21) Calculated free energy of deprotonation and ΔpK_a values at the N5 position of DHF bound in the closed form of *ec*DHFR and the average D-A distance for two independent free energy perturbation data sets are presented in Table S11.

2. Calculation of Kinetic Complexities.

The multistep nature of catalytic turnover (i.e. substrate binding, product release, conformational/protonation changes, etc.) results in what is known as kinetic complexity, which causes the observed KIEs to be smaller than their intrinsic values resulting from bond cleavage.(22-23) The relation between the observed KIE (KIE_{obs}) with the intrinsic value (KIE_{int}) is given by Eq. S5: (22-23)

$$KIE_{obs} = \frac{KIE_{\text{int}} + C_f + C_r EIE}{1 + C_f + C_r} \qquad \text{(S5)}$$

where EIE is the equilibrium isotope effect, and C_f and C_r are the forward and reverse commitments to catalysis, respectively. For the hydride transfer reaction catalyzed by *ec*DHFR under aerobic conditions, the $C_r \approx 0$ and the EIE is close to unity, because the reaction is very exothermic, oxygen consumes the product, and the H-isotope is bound to sp^3 carbon in both reactant and product states. Therefore, Eq. S5 can be simplified to Eq. S6:

$$KIE_{obs} = \frac{KIE_{\text{int}} + C}{1 + C} \qquad \text{(S6)}$$

where the commitment *C* is the commitment to catalysis,(22) which can be calculated from the observed and intrinsic KIEs obtained from Eqs. S2 and S3, respectively. The observed pre-steady state KIEs (denoted in the literature as ${}^{D}k_H$, k_H/k_D, k_{NADPH}/k_{NADPD}, or ${}^{D}k_{hyd}$) have been reported for *ec*DHFR at pH 9 and pH 7 (Figure S1A and S1B, respectively),(1-2) and it was suggested that the hydride transfer has temperature dependent KIEs at pH 7, but temperature independent KIEs at pH 9, in accordance with a different chemical mechanism at these pH regimes. In contrast to this interpretation, the comparison of the reported observed KIEs(1-2) and the intrinsic KIEs(24) and the calculation of *C* from Eq. S6 (Figure S1) reveal that the intrinsic KIEs are temperature independent at both high and low pH. However, the commitment to catalysis on the pre-steady state measurements is temperature dependent at pH 7, and temperature independent at pH 9 (Figure S6). Since the Arrhenius plot for this commitment (Figure S6C) is linear, it is reasonable to suggest that a single step, which is not the hydride transfer, is responsible for the different commitments at high and low pH. According to the data presented in Figure 2 and Table 1 in the main text, that step could be the protonation of N5 of DHF, which is part of the commitment at pH 7 but not at pH 9. The intrinsic KIEs for the hydride transfer, on the other hand, are temperature independent at all pH values.

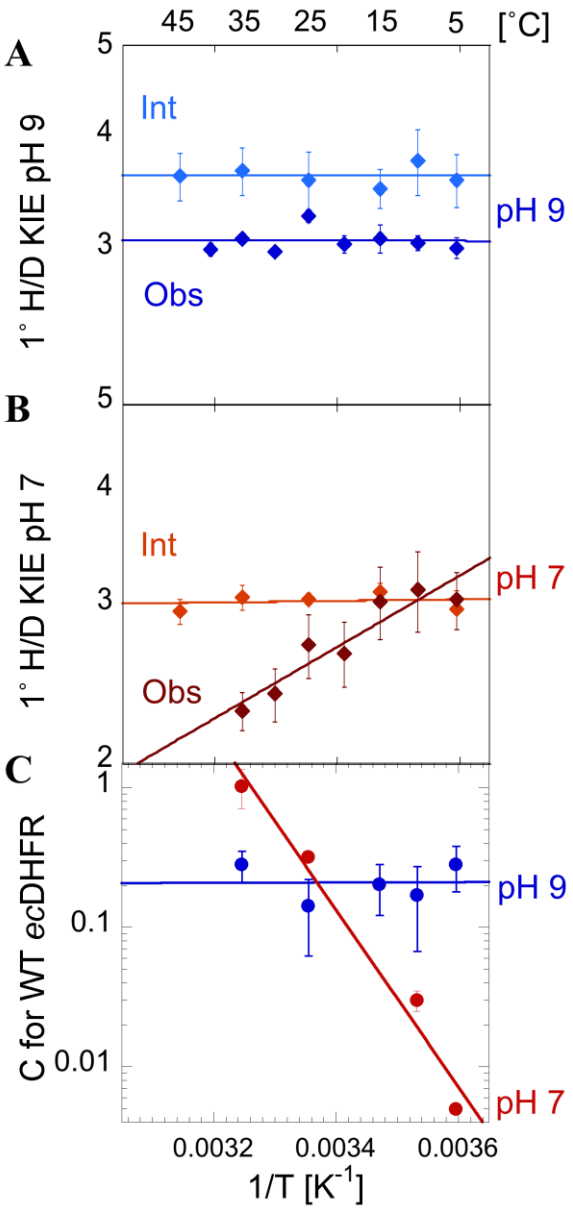

Figure S1. The relationship between observed KIE from pre-steady state measurements (KIE_{obs} in dark colors),(1-2) KIE_{int} (KIE_{int} in light colors),(24) and the commitment to catalysis for the observed KIEs (C) at pH 7 (blue) and pH 9 (red). **A)** Arrhenius plot for KIEs at pH 9; **B)** Arrhenius plots for KIEs at pH 7; **C)** Arrhenius plot for the commitment to catalysis for the pre-steady state KIEs at pH 7 and 9. All lines are the exponential fit to the Arrhenius equation (Eq. S4).

3. Steady-State vs. Pre-equilibrium Approximations.

$$\text{E:NADPH:DHF} + \text{H}^+ \underset{k_{\text{-prot}}}{\overset{k_{\text{prot}}}{\rightleftharpoons}} \text{E:NADPH:DHF-H}^+ \xrightarrow{k_{\text{hyd}}} \text{E:NADP}^+\text{:THF}$$

(Steady-State Approximation)

$$\frac{\text{d[P]}}{\text{dt}} = \text{k}_{\text{hyd}}*\left[\text{E:NADPH:DHF-H}^+\right] = \frac{(\text{k}_{\text{prot}})(\text{k}_{\text{hyd}})}{(\text{k}_{\text{-prot}})+(\text{k}_{\text{hyd}})}*[\text{E:NADPH:DHF}][\text{H}^+] \quad \frac{d[P]}{dt} = k_{hyd} *$$

$$\left[\text{E:NADPH:DHF-H}^+\right] = \frac{(k_{prot})(k_{hyd})}{(k_{-prot})+(k_{hyd})} * [\text{E:NADPH:DHF}][\text{H}^+] \qquad \text{(S7)}$$

(Pre-equilibrium Approximation)

$$\frac{d[P]}{dt} = k_{hyd} * \left[\text{E:NADPH:DHF-H}^+\right] = \frac{(k_{prot})(k_{hyd})}{(k_{-prot})} * [\text{E:NADPH:DHF}][\text{H}^+] \qquad \text{(S8)}$$

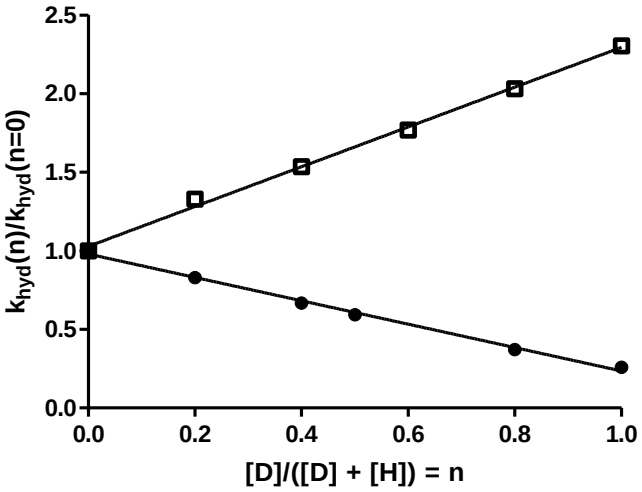

Figure S2. Proton Inventory plot of $k_{\text{hyd}}(n)/k_{\text{hyd}}(n=0)$ vs. [D]/([D]+[H]). The data points obtained at pL values of 5.3 (●) and 11.5 (□) were fitted to two separate straight lines.

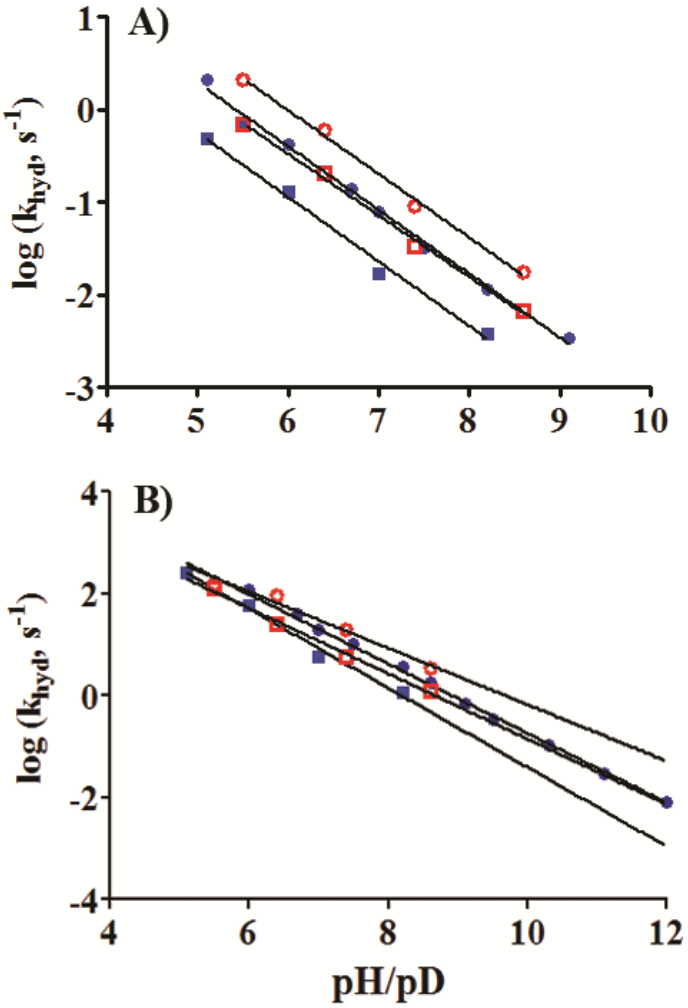

Figure S3. Plot of the log (k_{hyd}) vs. pH/pD for the various *ec*DHFR variants at 25 °C: A) D27S and B) Y100F. The data points are presented as: ● NADPH in H_2O; ○ NADPH in D_2O; ■ NADPD in H_2O; □ NADPD in D_2O. The parameters used for the fitted linear lines are given in Table S1.

It should be noted that the "sigmoidal" pH/rate profiles presented previously for ecDHFR hydride transfer reaction is strictly due to plotting the rates vs. pH/pD.(1) In other words the sigmoidal behaviors are purely artificial constructs that arises from plotting normal rate values (not log(rate)) vs. pH which is of log scale. When the same data are re-plotted (Figure S4) so that the x- and y- axes are of same scales (log scale), the sigmoidal shape disappears and kinetic behavior looks similar to that reported by Fierke *et. al.*(6)

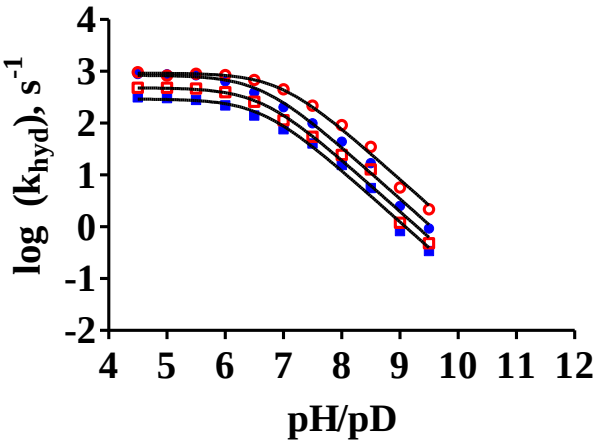

Figure S4. Re-plotting the k_{hyd} values vs. pH/pD for the WT *ec*DHFR promoted hydride transfer reaction at 25°C as reported in reference (1) (● NADPH in H_2O; ○ NADPH in D_2O; ■ NADPD in H_2O; □ NADPD in D_2O). The data were fit to the same expression described in ref. 9, which is a simplified form of eq. 1 when the k_2 constant (high pH plateau rate constant) is set to zero.

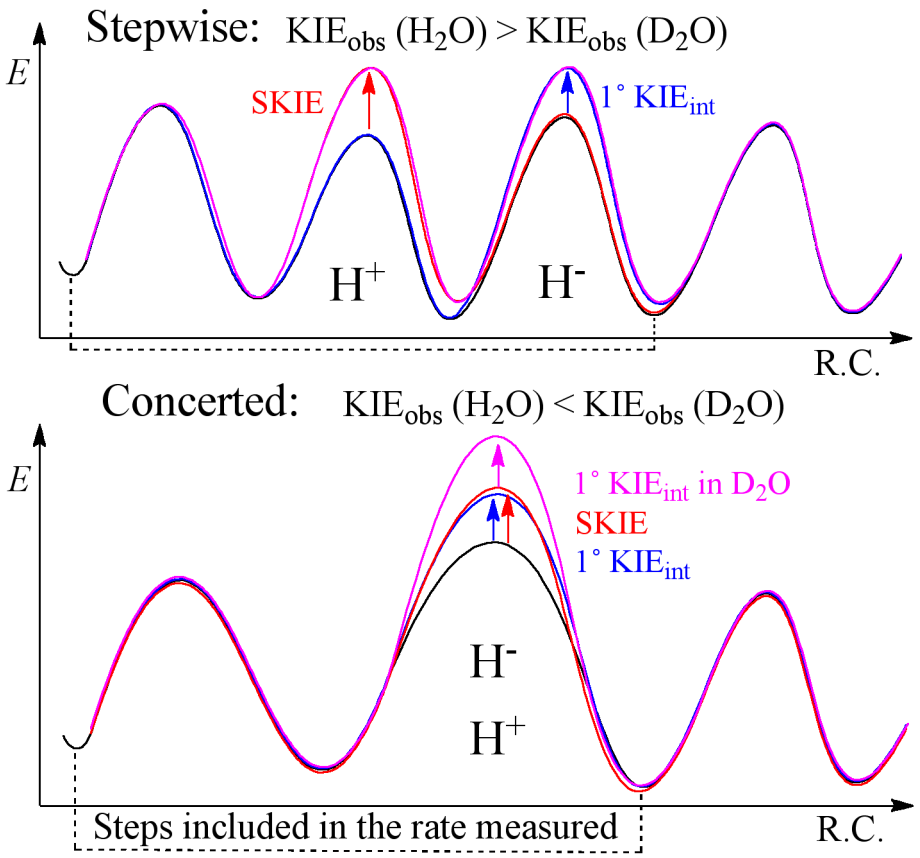

Figure S5 Kinetic outcomes from multiple isotope effects(30) depicted as energy diagrams along the reaction coordinate (**black**: H^+ and H^- transfers; **blue:** H^+ and D^- transfers; **red:** D^+ and H^- transfers; and **magenta:** D^+ and D^- transfers). The arrows mark the energy change between H and D transfers (leading to the different KIEs). The outcome in each panel is also true for SKIE with NADPH vs. NADPD, but for inverse SKIEs the red and magenta lines would represent H^+ transfer and the black and blue lines D^+ transfers, and the outcome would be reversed.

Table S1. Standard linear regression parameters used to fit the log (k_{hyd}) vs. pH/pD for the various *ec*DHFR variants in Figures 2 and S3.

*ec*DHFR constructs	slope (s^{-1} pL^{-1})	y-intercept (s^{-1})	r^2
D27S – NADPH in H_2O	- 0.69 ± 0.02	3.7 ± 0.1	0.9950
D27S – NADPH in D_2O	- 0.69 ± 0.03	4.1 ± 0.2	0.9961
D27S – NADPD in H_2O	- 0.70 ± 0.05	3.2 ± 0.3	0.9914
D27S – NADPD in D_2O	- 0.66 ± 0.03	3.5 ± 0.2	0.9960
Y100F – NADPH in H_2O	- 0.68 ± 0.01	6.1 ± 0.1	0.9968
Y100F – NADPH in D_2O	- 0.55 ± 0.06	5.4 ± 0.4	0.9777
Y100F – NADPD in H_2O	- 0.78 ± 0.06	6.4 ± 0.4	0.9871
Y100F – NADPD in D_2O	- 0.64 ± 0.03	5.6 ± 0.2	0.9943
D27S/Y100F – NADPH in H_2O	- 0.87 ± 0.03	3.5 ± 0.2	0.9947
D27S/Y100F – NADPH in D_2O	- 0.88 ± 0.07	4.0 ± 0.5	0.9881
D27S/Y100F – NADPD in H_2O	- 0.89 ± 0.09	3.3 ± 0.6	0.9809
D27S/Y100F – NADPD in D_2O	- 0.88 ± 0.09	3.5 ± 0.6	0.9804

Table S2. Summary of multiple isotope effects on the hydride transfer reaction promoted by the Y100F, D27S, and D27S/Y100F *ec*DHFR variants at 25 °C and various pL conditions.

pH or pD	**SKIE (NADPH) = k_{H2O}/k_{D2O}**	**SKIE (NADPD) = k_{H2O}/k_{D2O}**	**KIE (H_2O) = k_{NADPH}/k_{NADPD}**	**KIE (D_2O) = k_{NADPH}/k_{NADPD}**
Y100F				
8.20	0.47 ± 0.03	0.49 ± 0.03	3.2 ± 0.2	3.3 ± 0.2
7.00	0.66 ± 0.05	0.72 ± 0.06	2.4 ± 0.2	2.6 ± 0.2
6.00	0.89 ± 0.07	0.98 ± 0.07	1.9 ± 0.1	2.1 ± 0.1
5.10	1.15 ± 0.07	1.30 ± 0.09	1.6 ± 0.1	1.8 ± 0.1
D27S				
8.20	0.41 ± 0.03	0.29 ± 0.02	3.7 ± 0.3	2.6 ± 0.2
7.00	0.41 ± 0.03	0.32 ± 0.02	3.6 ± 0.2	2.8 ± 0.2
6.00	0.41 ± 0.02	0.34 ± 0.02	3.5 ± 0.2	3.0 ± 0.2
5.10	0.41 ± 0.04	0.37 ± 0.02	3.5 ± 0.2	3.1 ± 0.2
D27S/Y100F				
8.20	0.42 ± 0.03	0.52 ± 0.03	2.2 ± 0.2	2.7 ± 0.2
7.00	0.42 ± 0.02	0.55 ± 0.04	2.1 ± 0.2	2.7 ± 0.1
6.00	0.41 ± 0.02	0.56 ± 0.04	2.0 ± 0.1	2.7 ± 0.2
5.10	0.41 ± 0.03	0.57 ± 0.04	1.9 ± 0.1	2.7 ± 0.2

Table S3. List of k_{hyd} rates determined in the low and high pL plateaus (k_1 and k_2, respectively), and the pK_a values for the WT *ec*DHFR-catalyzed hydride transfer reaction at 25 °C. The values were obtained from fitting the data in Figure 2 to eq. 1, and the r^2 values from the fits are also given below.

	k_{hyd} at low pH, s^{-1}	k_{hyd} at high pH, s^{-1}	Kinetic pK_a	r^2
NADPH in H_2O	830 ± 70	0.13 ± 0.01	6.70 ± 0.05	0.9868
NADPH in D_2O	410 ± 30	0.23 ± 0.03	7.46 ± 0.05	0.9896
NADPD in H_2O	320 ± 20	0.048 ± 0.005	6.46 ± 0.05	0.9974
NADPD in D_2O	340 ± 30	0.09 ± 0.01	6.95 ± 0.06	0.9893

Table S4. Hydride transfer rates determined for the various *ec*DHFR variants and the computed ΔG values at 298.15 K. The ΔΔ$G^‡$ values are determined as the Δ$G^‡$ of the specific *ec*DHFR construct minus the Δ$G^‡$ (WT).

	k_{hyd} (s^{-1})	Δ$G^‡$ (kcal/mol)	ΔΔ$G^‡$ (kcal/mol)**
pH 7.0			
WT	280 ± 20	14.11± 0.04	0
Y100F	19.8 ± 0.8	15.68 ± 0.03	1.57 ± 0.05
D27S	0.082 ± 0.005	18.92 ± 0.07	4.81 ± 0.08
D27S/Y100F	0.0027 ± 0.0001	20.95 ± 0.02	6.84 ± 0.04
pH 9.0			
WT	4.3 ± 0.6	16.58 ± 0.09	0
Y100F	0.87 ± 0.08	17.53 ± 0.05	0.95 ± 0.10
D27S	0.00345 ± 0.00007	20.80 ± 0.01	4.22 ± 0.09
D27S/Y100F	(4.8 ± 0.2) E-05	23.33 ± 0.03	6.75 ± 0.09

* Δ$G^‡$ determined from the Eyring equation.

** propagated error = $(\delta X^2 + \delta Y^2)^{1/2}$, where δX and δY are the uncertainties associated with the compared Δ$G^‡$ values.

Table S5: Intrinsic and Observed KIEs of Y100F at pH 9.0[a]

T, °C	H/D Intrinsic	H/T Observed	D/T Observed
5	5.19 ± 0.09	3.607 ± 0.007	1.677 ± 0.005
15	5.10 ± 0.05	3.262 ± 0.018	1.627 ± 0.002
25	5.07 ± 0.07	2.912 ± 0.011	1.573 ± 0.012
35	4.98 ± 0.05	2.574 ± 0.008	1.510 ± 0.003
45	4.90 ± 0.09	2.305 ± 0.009	1.452 ± 0.015

[a] Observed KIEs were measured in 50 mM METN buffer. The values represent at least 5 independent measurements with their standard deviation.

Table S6: Intrinsic and Observed and KIEs of D27S at pH 9.0[a]

T, ºC	H/D Intrinsic	H/T Observed	D/T Observed
5	5.62 ± 0.16	2.15 ± 0.02	1.44 ± 0.01
15	5.30 ± 0.33	2.00 ± 0.01	1.39 ± 0.01
25	5.10 ± 0.21	1.77 ± 0.01	1.32 ± 0.01
35	4.94 ± 0.17	1.68 ± 0.01	1.29 ± 0.01
45	4.69 ± 0.35	1.53 ± 0.01	1.23 ± 0.01

[a] Observed KIEs were measured in 50 mM METN buffer. The values represent at least 5 independent measurements with their standard deviation.

Table S7: Intrinsic and Observed and KIEs of Y100F/D27S at pH 9.0[a]

T, ºC	H/D Intrinsic	H/T Observed	D/T Observed
5	6.09 ± 0.32	2.92 ± 0.01	1.62 ± 0.02
15	5.28 ± 0.24	2.61 ± 0.02	1.53 ± 0.02
25	4.71 ± 0.21	2.41 ± 0.01	1.47 ± 0.01
35	4.17 ± 0.35	2.29 ± 0.01	1.42 ± 0.01
45	3.57 ± 0.40	2.11 ± 0.01	1.35 ± 0.02

[a] Observed KIEs were measured in 50 mM METN buffer. The values represent at least 5 independent measurements with their standard deviation.

Table S8: Intrinsic and Observed and KIEs of WT pH 7.0[a]

T, ºC	H/D Intrinsic	H/T Observed	D/T Observed
5	2.99 ± 0.15	1.61 ± 0.02	1.22 ± 0.01
15	3.11 ± 0.06	2.64 ± 0.01	1.43 ± 0.01
25	3.05 ± 0.04	2.65 ± 0.02	1.43 ± 0.02
35	3.05 ± 0.10	2.65 ± 0.01	1.43 ± 0.01
45	2.95 ± 0.09	2.71 ± 0.01	1.43 ± 0.01

[a] Observed KIEs were measured in 50 mM METN buffer. The values represent at least 5 independent measurements with their standard deviation.

Table S9: C for observed KIEs from pre-steady state rates ($^{D}k_{hyd}$) from refs (2) and (1) for WT at pH 7.0 and pH 9.0

T, ºC	pH 7	pH 9
5	0.0050 ± 0.0004	0.283 ± 0.102
10	0.030 ± 0.005	0.171 ± 0.103
15		0.204 ± 0.081
25	0.32 ± 0.03	0.143 ± 0.080
35	1.03 ± 0.32	0.282 ± 0.073

Table S10. Partial charges for protonated and deprotonated DHF used in free energy calculations

Atom Name	q (DHF-H^+)	q (DHF)
N1	–0.652	–0.674
C2	0.775	0.737
N2	–0.936	–0.885
H21	0.453	0.397
H22	0.453	0.397
N3	–0.391	–0.494
HN3	0.348	0.359
C4	0.434	0.443
O4	–0.510	-0.551
C4A	–0.150	0.182
N5	–0.238	–0.528
HN5	0.378	0.000
C6	0.299	0.161
C7	0.084	0.021
H71	0.097	0.053
H72	0.097	0.053
N8	–0.469	–0.377
HN8	0.357	0.305
C8A	0.457	0.306
C9	0.066	0.046
H91	0.103	0.103
H92	0.103	0.103
N10	–0.686	–0.686
H10	0.373	0.373
C11	–0.090	–0.090
C12	–0.152	–0.152
H12	0.153	0.153
C13	–0.198	–0.198
H13	0.115	0.115
C14	0.260	0.260
C15	–0.198	–0.198
H15	0.104	0.104
C16	–0.152	–0.152
H16	0.186	0.186
C	0.692	0.692
O	–0.653	–0.653

N	–0.541	–0.541
HN	0.288	0.288
CA	0.074	0.074
HA	0.037	0.037
CT	0.799	0.799
O1	–0.809	–0.809
O2	–0.809	–0.809
CB	–0.011	–0.011
HB1	0.016	0.016
HB2	0.016	0.016
CG	–0.056	–0.056
HG1	–0.021	–0.021
HG2	–0.021	–0.021
CD	0.820	0.820
OE1	–0.846	–0.846
OE2	–0.846	–0.846

Table S11. Calculated free energy of deprotonation and ΔpK_a values at the N5 position of DHF bound in the closed form of *ec*DHFR and the average D-A distance for two independent free energy perturbation data sets

	Data Set 1	Data Set 2
ΔA Tyr100 Protonated [kcal/mol]	–11.41 ± 0.42	–12.35 ± 0.40
ΔA Tyr100 Deprotonated [kcal/mol]	–5.33 ± 0.82	–5.97 ± 0.52
ΔpK_a	4.7	4.9
<D-A> Tyr100 Protonated [Å]	3.7 ± 0.2	3.7 ± 0.3
<D-A> Tyr100 Deprotonated [Å]	3.6 ± 0.2	3.5 ± 0.2

6. References

1. Loveridge EJ, Allemann RK (2011) Effect of pH on hydride transfer by Escherichia coli dihydrofolate reductase. *Chembiochem* 12(8):1258-1262.
2. Loveridge EJ, Behiry EM, Swanwick RS, Allemann RK (2009) Different reaction mechanisms for mesophilic and thermophilic dihydrofolate reductases. *J Am Chem Soc* 131(20):6926-6927.
3. Blakley RL (1960) Crystalline Dihydropteroylglutamic Acid. *Nature* 188(4746):231-232.
4. Sen A, Stojković V, Kohen A (2012) Synthesis of Radiolabeled Nicotinamide Cofactors from Labeled Pyridines: Versatile Probes for Enzyme Kinetics. *Anal. Biochem.* 430(2):123-129.
5. Welsh KM, Creighton DJ, Klinman JP (1980) Transition-state structure in the yeast alcohol dehydrogenase reaction: the magnitude of solvent and alpha-secondary hydrogen isotope effects. *Biochemistry* 19(10):2005-2016.

6. Fierke CA, Johnson KA, Benkovic SJ (1987) Construction and evaluation of the kinetic scheme associated with dihydrofolate reductase from Escherichia coli. *Biochemistry* 26(13):4085-4092.
7. Melander L, Saunders WH eds (1987) *Reaction Rates of Isotopic Molecules* (Krieger, R.E., Malabar, Fl), 4 Ed.
8. Sen A, Yahashiri A, Kohen A (2011) Triple isotopic labeling and kinetic isotope effects: exposing H-transfer steps in enzymatic systems. *Biochemistry* 50(29):6462-6468.
9. Stojkovic V, Perissinotti LL, Willmer D, Benkovic SJ, Kohen A (2012) Effects of the donor-acceptor distance and dynamics on hydride tunneling in the dihydrofolate reductase catalyzed reaction. *Journal of the American Chemical Society* 134(3):1738-1745.
10. Wang L, Goodey NM, Benkovic SJ, Kohen A (2006) Coordinated effects of distal mutations on environmentally coupled tunneling in dihydrofolate reductase. *Proc Natl Acad Sci U S A* 103(43):15753-15758.
11. Kohen A, Limbach HH eds (2006) *Isotope Effects in Chemistry and Biology* (CRC Press, Taylor and Francis, Boca Raton, Fl).
12. Cornell WD, *et al.* (1996) A second generation force field for the simulation of proteins, nucleic acids, and organic molecules (vol 117, pg 5179, 1995). *Journal of the American Chemical Society* 118(9):2309-2309.
13. Hornak V, *et al.* (2006) Comparison of multiple amber force fields and development of improved protein backbone parameters. *Proteins: Structure, Function, and Bioinformatics* 65(3):712-725.
14. Jorgensen WL, Chandrasekhar J, Madura JD, Impey RW, Klein ML (1983) Comparison of Simple Potential Functions for Simulating Liquid Water. *Journal of Chemical Physics* 79(2):926-935.
15. Wang JM, Wolf RM, Caldwell JW, Kollman PA, Case DA (2004) Development and testing of a general amber force field. *Journal of Computational Chemistry* 25(9):1157-1174.
16. Case DA, *et al.* (2010) AMBER 11 (University of California, San Francisco).
17. Sawaya MR, Kraut J (1997) Loop and subdomain movements in the mechanism of Escherichia coli dihydrofolate reductase: crystallographic evidence. *Biochemistry* 36(3):586-603.
18. Nose S (1984) A Molecular-Dynamics Method for Simulations in the Canonical Ensemble. *Molecular Physics* 52(2):255-268.
19. Hoover WG (1985) Canonical Dynamics - Equilibrium Phase-Space Distributions. *Physical Review A* 31(3):1695-1697.
20. Parrinello M, Rahman A (1980) Crystal-Structure and Pair Potentials - a Molecular-Dynamics Study. *Physical Review Letters* 45(14):1196-1199.
21. Van Gunsteren WF, Berendsen HJC (1988) A Leap-Frog Algorithm for Stochastic Dynamics. *Molecular Simulation* 1(3):173-185.
22. Cook PF, Cleland WW (2007) *Enzyme kinetics and mechanism* (Taylor & Francis Group LLC, New York, NY).
23. Northrop DB (1991) Intrinsic isotope effects in enzyme catalyzed reactions. *Enzyme mechanism from isotope effects*, ed Cook PF (CRC Press, Boca Raton, Fl.), pp 181-202.
24. Francis K, Stojkovic V, Kohen A (2013) Preservation of Protein Dynamics in Dihydrofolate Reductase Evolution. *J Biol Chem*.